Static and Dynamic Stability of a Polar Ship in the Arctic Region with Ice Accumulation

Jianzhang Qi[1, 2], Wei Chai[1,2*], Chana Sinsabvarodom[3], Meng Cui[4], Xiaoliang Dou[4], Tiantian Zhu[5], Shunying Ji[6]

1. Key Laboratory of High Performance Ship Technology (Wuhan University of Technology), Ministry of Education, Wuhan, China.

2. School of Naval Architecture, Ocean and Energy Power Engineering, Wuhan University of Technology, Wuhan, 430063, China.

3. Department of Civil Engineering, Chiang Mai University, Chiang Mai, Thailand

4. Marine Design & Research Institute of China, Shanghai, 200011, China

5. Department of Technology and Safety, UiT-the Arctic University of Norway

6. State Key Laboratory of Structural Analysis, Optimization and CAE Software for Industrial Equipment, Dalian University of Technology, Dalian 116023, China

Abstract: The harsh and complex marine environment of the Arctic region poses significant challenges for polar ships, particularly in cases where ice accumulates on ship surfaces, which can severely influence vessel stability. This study presents a comprehensive analysis of both static and dynamic stability for a polar ship subjected to ice accumulation, a topic of critical scientific importance and engineering relevance for ensuring the safety of Arctic navigation. Specifically, a simplified model for predicting ice accumulation weight is proposed, which uses the spray rate, icing coefficient, and hull area segmentation to facilitate accurate and efficient forecasting of ice accumulation on ships. The effects of ice accumulation on the static stability of a polar ship during several different hours of icing events are compared with those of a no-ice case under typical marine meteorological and hydrological environmental conditions, and the requirements in the IMO IS code are verified. Additionally, to evaluate dynamic stability, a roll motion mathematical model is developed to predict the roll response of a polar ship with ice accumulation, with roll damping parameters obtained via free-decay computational fluid dynamics (CFD) simulations. Furthermore, the average conditional exceedance rate (ACER) method is applied to conduct an extreme value analysis of the roll response under the action of wind and waves, enabling a thorough assessment of the ultimate dynamic stability with ice accumulation. This study systematically analyzes the stability loss of a polar ship induced by ice accumulation, which can contribute to the design of polar equipment and the safety of polar navigation.

*Corresponding author.

E-mail address: chaiwei@whut.edu.cn (Wei Chai).

Keywords: Polar ship; Ice accumulation; Extreme value analysis; Ship stability; Roll motion.

Nomenclature

Alphabetical Symbols

GZ	Righting arm
GM	Metacentric height
$\omega(z)_{\text{wind}}$	Quantity of wind-driven spume
$\omega(z)_{\text{wave}}$	Quantity of breaking wave spume
h_s	Significant wave height
z	Height above the ship's deck
ω_0	Empirical constant
Ψ	Empirical constant
U_{10}	Wind speed at an altitude of 10 meters
v_{sw}	Relative velocity between ship and waves
t_w	Significant wave period
α	Angle between the ship's heading and wind direction
v_s	Ship speed
$\dot{M}_{w,t}$	Total droplet spray rate
$\dot{M}_{w,wind}$	Droplet spray rate of wind
$\dot{M}_{w,wave}$	Droplet spray rate of wave
B_s	Shape coefficient
E	Collision efficiency
n_{ice}	Ice accumulation coefficient
ρ_{i}	Density of ice
L_{f}	Latent heat of ice melting
σ_{M}	Interface distribution coefficient
h_{c}	Heat transfer coefficient
T_{w}	Temperature at the seawater–air interface
T_{a}	Air temperature

p	Air pressure
e_s	Saturation vapor pressure
RH	Relative humidity of the air
c_w	Specific heat capacity of seawater
T_d	Droplet temperature
σ	Stefan-Boltzmann constant
a_Q	Linearization constant of radiative heat flux
$\dot{M}_{ice}$	Icing rate per hour per unit area
t_i	Duration of the ice accumulation process
S1	Deck
S2	Horizontal areas of the superstructure
S3	Ship sides
S4	Vertical areas of the superstructure
S_{Sn}	Area of different regions
$M_{ice}(Sn)$	Weighted average ice accumulation rate for regionsSn
M_t	Total weight of ice accumulation
I_{44}	Roll moment of inertia
A_{44}	Additional roll moment of inertia
φ_t	Roll angle at time *t*
$\dot{\varphi}_t$	Roll angular velocity at time *t*
$\ddot{\varphi}_t$	Roll angular acceleration at time *t*
B_{44}	Linear roll damping term
B_{44n}	Nonlinear roll damping term
$M_{wave}(t)$	Random irregular wave-induced moment
$M_{wind}(t)$	Wind heeling moment
$\gamma(\omega_n)$	Effective wave slope coefficient
ζ_t	Waveform function
N_w	Number of irregular waves
k_w	Wavenumber~~Wave number~~

ξ_{An}	Wave amplitude for regular waves
ω_n	Wave frequency
ε_n	Random phase angle
$S(\omega_n)$	Wave spectrum
ρ_{air}	Air density
A_L	Lateral wind-exposed area of the ship
C_y	Wind moment coefficient
H_w	Vertical distances from the waterline plane to the wind field center of the action
H_{yd}	Vertical distances from the waterline plane to the wave force center of the action
$\overline{V_w}$	Steady wind speed
K	Constant of the Davenport gust spectrum
$V_g(t)$	Gusting wind speed
$\overline{u_i}, \overline{u_j}$	Averaged velocity vectors of flow
x_i	Cartesian coordinates
$\bar{p}$	Mean pressure
ρ	Fluid density
$\overline{\acute{u_i}\acute{u_j}}$	Negative value of Reynolds stresses
$\overline{\tau_{ij}}$	Mean viscous stress tensor components
ν	Coefficient of fluid viscosity
u_t	Turbulent eddy viscosity
ke	Turbulent kinetic energy
δ_{ij}	Kronecker delta
a_r	Linear decay coefficient
b_r	Nonlinear decay coefficient
$\Delta\varphi_A$	Difference between the amplitudes of two consecutive half-cycles
φ_{Am}	Average value of adjacent amplitude values
T_r	Natural period of polar ship roll motion
Q	Number of peak values of roll motion within 50 hours
k	Order of the ACER function

$\hat{\varepsilon}_k(\eta)$	Empirical ACER function of order k
a_k, b_k, c_k and q_k	Constants related to the order k
η_i	Estimated extreme level of the empirical ACER function
ρ_i	Weight factor that assigns higher weights to reliable data points
λ	Exceedance probability
t_{all}	Total duration of the jet per minute
L_{OA}	Overall length
B	Beam
d	Draft
∇	Volumetric displacement
Δ	Displacement
g	Gravity acceleration
GM_0	GM with no ice
GM_{6h}	GM with 6 h ice

1 Introduction

The Arctic region, with its unique geographic advantages and abundant natural resources such as fisheries, oil, gas, and minerals, has garnered significant international attention (Chai W, 2018). As global climate change results in a reduction in Arctic Sea ice coverage, the feasibility of polar navigation has increased because of reduced transportation time and costs. Arctic nations are proposing various related projects and research efforts to promote the development of ships capable of operating in polar environments.

The distinctive geographic location in the Arctic creates harsh climatic conditions with factors such as large waves, strong winds, sea fog, and low temperatures, as a result, pose threats to polar ships. Low temperatures can impact the operation of marine equipment and the physical properties of steel structures. Ice accumulation due to sea waves raises the center of gravity of ships, thereby reducing their stability. Above the waterline, ships are affected by wind loads, which can cause listing and exacerbate the freezing of seawater spray on the ship, posing a serious threat to navigation safety (Mintu, 2022). Ice accumulation presents an even greater risk to medium-sized and small ships, as demonstrated by the sinking of the Russian fishing ship "Onega" in the Barents Sea in 2020. The incident, caused by inadequate ice removal, resulted in ship capsizing and led to 17 casualties. Research on the stability assessment of ships under the combined action of ice accumulation and waves, revealing the stability losses that may cause ship capsizing due to ice accumulation, has important scientific significance and engineering value for ensuring the safety of navigation.

Accurate forecasting is essential for assessing the threat posed by ice accumulation to the stability of polar ships. The rate of ice accumulation varies with factors such as temperature, wind speed, and other environmental conditions, and key forecasting methods include empirical statistical models, physical models, and numerical simulations. Research on ship icing prediction began as early as 1955, following incidents of icing on the "Lorella" and "Rodrigo" trawlers in Iceland's northern fishing grounds (Dehghani-Sanij A. R. et al., 2017). Early studies relied primarily on the inductive analysis of ship monitoring data and environmental input parameters, employing semiquantitative methods on the basis of the statistical relationship between the severity of ship icing and environmental conditions (Zhang Y et al., 2023). However, ensuring universal applicability across different ship types and marine environments has proven challenging. In response, researchers have attempted to simulate the physical phenomena of ship icing directly. In 1983, the Norwegian Hydrodynamic Laboratory developed the first physical ice accumulation model, ICEMOD, by Horjen (1986). This model has several limitations, such as setting

the freezing coefficient (the ratio of water flux freezing into ice to the water flux acting on the structure) at 0.5, which does not accurately reflect real conditions. Recent updates by Horjen have addressed these issues by incorporating calculations for heat transfer through ice on the basis of time-varying temperature distributions (Horjen, 2023) and supercooled droplet assumptions (Horjen, 2024). Additionally, numerous researchers have explored areas such as spray dynamics (Shafiul Mintu, 2021; Sushmit Dhar, 2024) and microscopic physical processes (Adarsh Dash, 2021; Shahla Ahmadi, 2022) to enhance ship icing prediction. These advancements, while offering more accurate representations of the icing process, also require greater computational resources. Achieving a balance between computational accuracy and resource efficiency for fast and precise predictions remains a critical challenge in the development of ice accumulation prediction models for polar ship stability research.

Ice accumulation adversely affects the static and dynamic stability of polar ships and may ultimately lead to capsizing under wind and wave action. A comprehensive stability assessment is needed to ensure the safety of polar ships exposed to accumulated ice. In a complex polar environment, ice accumulation increases a ship's displacement and increases its center of gravity, which reduces the righting arm (GZ) and metacentric height (GM), ultimately leading to a loss of static stability (DeNucci T, 2024). Numerous studies have explored the impact of ice on a ship's static stability (Johansen K., 2020), and relevant guidelines and regulations have been established (IMO, 2003; 2014). For dynamic stability, there is still insufficient quantitative evaluation for polar ships in winds and waves, particularly under dead ship conditions of dangerous stability failure. Dead ship stability is a key focus in the development of the International Maritime Organization (IMO) second-generation intact stability standards. Researchers often simplify and solve the differential equations governing heave motion via a segmented linearization method (Silva K M., 2021) and study the nonlinear system characteristics through the Melnikov equation (Wang Y, 2023), Lyapunov exponents (Ucer. E, 2019), and safe basin theory (Liu, 2019). Current research on the stability of polar ships with ice accumulation has focused primarily on static stability, with comparatively less focus on dynamic stability and a limited understanding of comprehensive stability loss assessments under wind and wave conditions.

The motion of ships under the action of wind and waves is characterized by significant randomness, and comprehensive dynamic stability analysis requires a large number of data samples. Probability forecasting methods can forecast extreme roll angles that occur with low probability, thereby providing a deeper evaluation of the stability of polar ships with ice accumulation. Early research on extreme value prediction of stochastic processes relied primarily on the study of maximum value distributions in traditional extreme value statistical theory, with

three types of maximum value distributions, specifically generalized extreme value distribution (GEV) models, being widely applied (Rypkema D and Tuljapurkar S,2021; Afzal M S., et al., 2023). In the context of ship roll motion as a random process, commonly used methods include the block maximum (BM) method (Zhou X, et al., 2023; Dombry C, 2019), which segments the random process and fits the distribution of the sequence of maximum values, and the peaks over threshold (POT) method (Pipiras V, 2020), which employs the generalized Pareto distribution (GPD) to model the distribution of peak values exceeding a specified threshold. The average conditional exceedance rate (ACER) method, proposed by Naess (Naess A, Gaidai O, Karpa O, 2013), is applicable to extreme value prediction for non-Gaussian and non-narrowband processes and can effectively predict extreme ship roll values, demonstrating greater robustness in scenarios with insufficient data or high data dependency. It is highly effective in predicting extreme events in complex systems, such as extreme motion responses in ship dynamics. However, considering the influence of ice accumulation on the ship roll motion response, the prediction of extreme roll values remains underexplored in current research on polar ship stability.

In summary, current ice prediction methods continue to face challenges in achieving a balance between accuracy and efficiency. Systematic research on the static and dynamic stability assessment of polar ships under the influence of ice accumulation is lacking, and a gap persists in the study of the ultimate stability of polar ships under such conditions. Accurately predicting while maintaining efficiency, along with the precise calculation and analysis of changes in static and dynamic stability under ice conditions and the exploration of ultimate stability in wind and wave environments, remains critical for assessing the risks posed by ice accumulation to polar ships.

This study aims to systematically evaluate the static and dynamic stability of a polar ship with ice accumulation under wind and wave action in the Arctic region. An efficient ship icing prediction model is developed by simplifying the classic Marine Icing model for the Norwegian COast Guard (MINCOG) model. Under typical meteorological and hydrological conditions, the variations in ship static stability parameters caused by ice accumulation over different durations are calculated, and the critical thresholds are determined on the basis of the requirements of the IMO IS Code. The dynamic stability is assessed via a ship motion model to evaluate changes in the roll motion response. Finally, the ACER method is employed to analyze extreme values of the roll angle and assess the ultimate dynamic stability of the polar ship with ice accumulation.

2 Ice accumulation model

The primary origin of ice accumulation on polar ships stems from the freezing of spray droplets at cold

temperatures. Factors such as ship motion, local meteorological conditions, and hydrological settings influence the rate of ice accumulation, which creates the risk to capsize in special extreme cases, as shown in Fig. 1 (Kubat I, 2005). Therefore, calculations of ship ice accumulation require complex multiphase fluid dynamics computations of seawater spray mass and thermodynamic calculations of spray freezing. To address this complexity, this study proposes a simplified ice accumulation prediction method based on the MINCOG model, inspired by the work of some scholars and relevant standards (Samuelsen et al., 2017; Makkonen L, 1987; Stallabrass J R, 1980; Horjen I, 1986). The study subsequently applies this method to compute ice accumulation on a specific polar ship under typical operational scenarios, aiming to further investigate its impact on ship stability in roll motion.

Fig. 1 A case of ice accumulation event in Arctic regions (Kubat I, 2005).

2.1 Theoretical background

The primary sources of ship icing from spray droplets originate from wind-driven spumes and breaking wave spumes, resulting from sustained wind and ship-generated wave interactions, respectively.

The quantity of wind-driven spumes is estimated via an empirical formula proposed by Preobrazhenskii (Preobrazhenskii L Y, 1973):

$$\omega(z)_{\text{wind}}=\omega_0\exp[-\Psi(z-\frac{h_s}{2})] \tag{1}$$

where h_s is the significant wave height (m), z is the height above the deck (m), and ω_0 and Ψ are empirical constants determined from various wind speeds at an altitude of 10 m U_{10}:

$$\omega_0=10^{-7}\ \text{kg/m}^3, \Psi=0.35(U_{10}=7\sim12\ \text{m/s})$$
$$\omega_0=10^{-5}\ \text{kg/m}^3, \Psi=1.00(U_{10}=15\sim25\ \text{m/s}) \quad (2)$$

For breaking wave spumes, the mass density of spray droplets generated by ship–wave collisions during transit is calculated via a formula summarized by Lozowski (Lozowski et al., 2000):

$$\omega(z)_{\text{wave}}=6.46\times10^{-5}h_s v_{sw}^2\exp(-\frac{z}{1.82}) \quad (3)$$

$$v_{sw}=1.56t_w+v_s\cos(\pi-\alpha)) \quad (4)$$

where v_s is the ship speed (m/s), v_{sw} is the relative velocity between the ship and waves, α is the angle between the ship's heading and wind direction (rad), and t_w is the significant wave period (s).

The total droplet spray rate $\dot{M}_{w,t}$ per minute, considering both wind-driven and breaking wave spumes, is expressed as:

$$\dot{M}_{w,t}=\dot{M}_{w,wind}+\dot{M}_{w,wave}=B_s E\alpha[\omega(z)_{\text{wind}}\cdot t_{all}+\omega(z)_{\text{wave}}\cdot 60] \quad (5)$$

where $\dot{M}_{w,wind}$ and $\dot{M}_{w,wave}$ are the droplet spray rates of wind and waves, respectively; B_s denotes the shape coefficient; and E represents the collision efficiency. In accordance with previous research (Horjen I, 1984), B_s and E have a value of 1 under pessimistic estimation, and t_{all} represents the total duration of the jet per minute, which can be calculated via the following formula:

$$t_{all}=\frac{10v_{sw}h_s}{U_{10}^2}\left[15.78\text{-}18.04\exp\left(-\frac{4.26v_{sw}}{1.56t_w^2}\right)\right] \quad (6)$$

After the droplet mass is calculated, the thermodynamic energy balance must be considered, which expresses the icing rate via the ice accumulation coefficient n_{ice}. Calculations for thermal equilibrium at the ice/water and air/water interfaces are performed via substitution into the heat balance equation, yielding:

$$\rho_i L_f(1\text{-}\sigma_M)n_{ice}M_w=h_c(T_w\text{-}T_a)+1731\frac{h_c}{p}(e_s(T_w)\text{-}RHe_s(T_a))+M_w c_w(T_w\text{-}T_d)+\sigma a_Q(T_w\text{-}T_a) \quad (7)$$

where ρ_{i} is the density of ice (kg/m³), L_{f} is the latent heat of ice melting (J/kg), σ_{M} is the interface distribution coefficient, h_{c} is the heat transfer coefficient (W/(m²·K)), T_{w} is the temperature at the seawater–air interface (K), T_{a} is the air temperature (K), p is the air pressure (kPa), e_{s} is the saturation vapor pressure (kPa), RH is the relative humidity of air, c_{w} is the specific heat capacity of seawater (J/(kg·K)), T_{d} is the droplet temperature (K), σ is the Stefan–Boltzmann constant (W/(m²·K⁴)), and a_Q is a linearization constant of radiative heat flux. The specific parameter values and calculation methods are described in Dehghani-Sanij's study (Dehghani-Sanij et al., 2016).

Once the spray rate $\dot{M}_{w,t}$ and the icing coefficient n_{ice} are obtained, the icing rate $\dot{M}_{ice}$ per hour per unit area can be computed:

$$\dot{M}_{ice} = n_{ice} \cdot 60 \cdot \dot{M}_{w,t} \tag{8}$$

In the simplified approach adopted in this study, the icing coverage area of the ship is divided into horizontal and vertical surfaces for calculating ice accumulation instead of discretizing the ship into tens of thousands or even hundreds of thousands of grids for individual solving. This significantly streamlines the computation, eliminating the requirements for complex three-dimensional modeling and processing.

The horizontal surfaces primarily encompass the deck and upper structure planes, whereas the vertical surfaces include the ship's sides and vertical areas of the upper structures. This approach references Ice Case 1 from the IMO guidelines, which assumes ice accumulation over all timber deck areas of the ship. According to relevant research, significant differences exist in the ice accumulation rates on the horizontal and vertical surfaces of ships. To account for these variations, the simplified method proposed and utilized in this paper draws from specifications on icing rates in the Polar Code (IMO, 2015). In the calculation, it is assumed that the ice accumulation rates on horizontal surfaces S1 (deck) and S2 (horizontal areas of the superstructure) are four times greater than those on vertical surfaces S3 (ship sides) and S4 (vertical areas of the superstructure). Taking a typical polar ship as an example, the division of ice accumulation areas is demonstrated in Fig. 2.

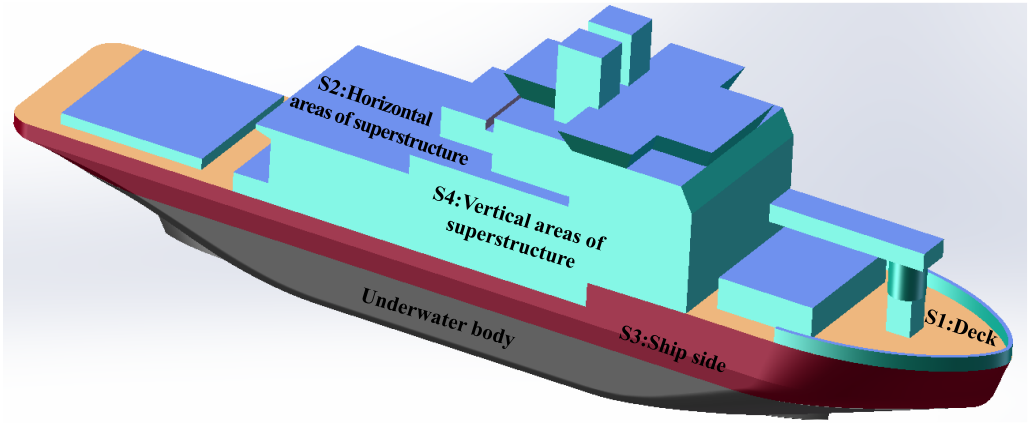

Fig. 2 Division of ice accumulation areas.

Next, the total weight of ice accumulation on the ship over a specified time period M_t is computed by averaging the M_{ice} values for different ship areas, weighted by their respective surface areas and ice accumulation times. Specifically:

$$M_t = [M_{ice}(\mathrm{S1}) \cdot S_{\mathrm{S1}} + M_{ice}(\mathrm{S2}) \cdot S_{\mathrm{S2}} + M_{ice}(\mathrm{S3}) \cdot S_{\mathrm{S3}} + M_{ice}(\mathrm{S4}) \cdot S_{\mathrm{S4}}\,] \cdot t_i \quad (9)$$

where t_i is the duration of the ice accumulation process (hour), $M_{ice}(Sn)$ represents the weighted average ice accumulation rate for region Sn, and S_{Sn} denotes the area of different regions Sn, with n= 4 in this study dividing the ship's area into S1 (deck horizontal), S2 (upper structure horizontal), S3 (side vertical), and S4 (upper structure vertical). For ships with complex upper structure and deck configurations, a finer division of areas should be employed to increase the accuracy of rapid ice accumulation forecasting.

2.2 Ice accumulation prediction

A typical polar ship is utilized for the calculation of ice accumulation and the prediction of roll motion responses. This study employs a simplified method based on the MINCOG model to compute the ice accumulation of this polar ship, with the delineation of its various regions illustrated above Fig. 2.

To better illustrate and assess the impact of ice accumulation on the roll stability of polar ships under harsh polar environmental conditions, it is necessary to extract the typical ice accumulation scenarios for the polar ship. On the basis of the research of Samuelsen et al., the typical ice accumulation condition is selected from observational data of KV Nordkapp (Samuelsen et al., 2015) and the Norwegian Reanalysis 10 km (NORA10) (Orimolade et al., 2016). The locations of ice accumulation events are shown in Fig. 3.

Fig. 3 Locations of ice accumulation events.

The ice accumulation calculation is consistent with the conditions used in the roll motion response calculation of the polar ship. The parameter selection is shown in Table 1. The calculated ice accumulation for the polar ship

using these parameters is summarized in Table 2.

Table 1 Parameter selection for ice accumulation prediction.

Parameters	**Symbols**	**Value**	**Units**
Empirical constants	Ψ	1	-
	ω_0	10^{-5}	kg/m3
The average height of droplets above the deck	z	8.8	m
Significant wave height	h_s	5.5	m
significant wave period	t_w	14	s
Ship speed	v_s	0	m/s
Wind speed (10 meters height)	U_{10}	20.6	m/s
Air temperature	T_a	-13.8	°C
Angle between wind speed and ship speed	α	0	rad

Table 2 The calculated ice accumulation of the polar ship.

	Region	Area m^2	hourly ice density kg/m^2	Ice accumulation weight kg	Ice/Ship Weight Ratio
Vertical	Superstructure	3676.6	12.3	391630.2	9.15%
	Side	1632.1			
horizontal	Superstructure	2193.4	49.2	873771.6	
	Deck	767.7			

On the basis of the calculation results, under severe environmental conditions, the polar ship accumulates a significant amount of ice within just 6 hours, with the ice weight ratio reaching 9.15%. Under actual sailing conditions, crew members typically remove ice from the deck and superstructure promptly to prevent excessive ice buildup, which could endanger the ship's stability. However, in extremely harsh marine environments, it may be challenging to clear ice, potentially leading to reduced static and dynamic stability. This could result in extreme roll angles exceeding threshold values, thereby increasing the risk of accidents, as observed in incidents**.** Therefore, evaluating the extreme roll stability of polar ships under ice accumulation conditions is crucial.

3 Roll motion of a polar ship with ice accumulation

A typical polar ship is selected as the research subject in this study because of its extensive navigation in both the Antarctic and Arctic regions, making its stability assessment under ice accumulation conditions of unquestionable practical significance. The ship's three-dimensional model is illustrated in Fig. 4.

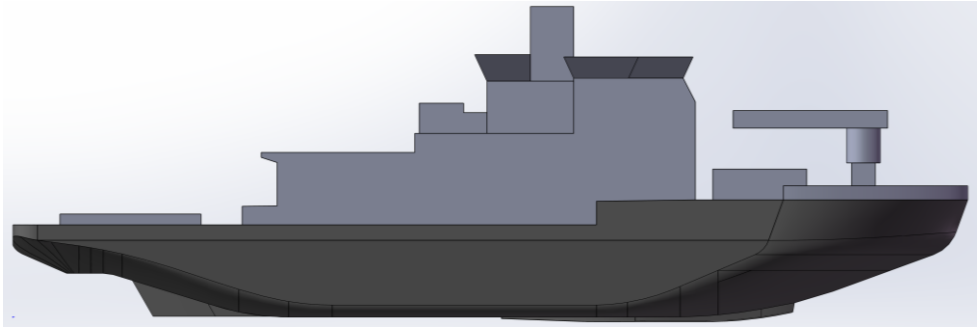

Fig. 4 Geometry of the polar ship.

Table 3 presents the main dimensions of the polar ship. The influence of the free liquid surface within the ship cabin is considered when the calculation parameters are determined. The method of correcting the free liquid surface involves using the center-of-gravity lifting technique.

Table 3 Major parameters of the polar ship.

Parameters	Symbols	Units	Model	Full-scale
Overall length	L_{OA}	m	2.08	125.5
Beam	B	m	0.39	23.2
Draft	*d*	m	0.13	7.785
Displacement	Δ	kg	64.052	$1.383*10^7$
Metacentric height (free surface correction)	*GM*	m	0.0125	0.75
Roll moment of inertia (free surface correction)	I_{44}	$kg*m^2$	1.334	$1.046*10^9$

3.1 Static stability of the ship with ice accumulation

The accumulation of ice on the hulls of ships can significantly alter their static stability. By analyzing changes in the GM and GZ curves, the impact of ice accumulation on the stability of the polar ship can be partially assessed. Using the calculated ice accumulation from Section 2.2, a comparison is made between the static stability of the polar ship under No-ice condition and 6h ice accumulation condition.

The GM value is a key parameter for reflecting a ship's static stability. Compared with the No-ice condition where GM_0 = 0.75 m, the selected 6h ice accumulation condition yields a reduced metacentric height of GM_{6h} =

0.34 m. Simultaneously, the decrease in the GM value indicates a weakening of the restoring force in the polar ship, resulting in slower recovery after inclination. Consequently, this often leads to an increase in the ship's natural period, causing the rolling motion to become more moderate. However, the reduced restoring capability may result in insufficient ship stability, which can even pose a risk of capsizing. This substantial decrease in metacentric height highlights the negative impact of ice accumulation on the initial stability of the polar ship but cannot perfectly reflect the stability with ice accumulation.

The GZ reflects the moment generated to restore the ship to its upright position when inclined under external forces due to the misalignment of the centers of gravity and buoyancy along the same vertical line. The righting arm plays a significant role in determining the ship's stability. Ice accumulation can lead to changes in the restoring arm of a ship, which may result in insufficient restoring forces during severe motions. This inadequacy could cause the ship to exceed its critical angle of heel and potentially capsize. Therefore, thoroughly assessing the impact of ice on the GZ of the polar ship is essential.

In this work, the GZ curves are computed for the No-ice case and several cases with different ice accumulation durations, as depicted in Fig. 5. The brown bars represent one of the stability criteria specified in the IS Code, which states that the GZ at a heel angle of 30° must not be less than 0.2 meters. When the GZ value at 30° falls below the height of the brown bars, the GZ curve of the corresponding icing condition does not meet the requirements specified by the IS Code. Additionally, the IS Code (2008) provides specific requirements for the area under the GZ curve, further details of which can be found in the referenced document.

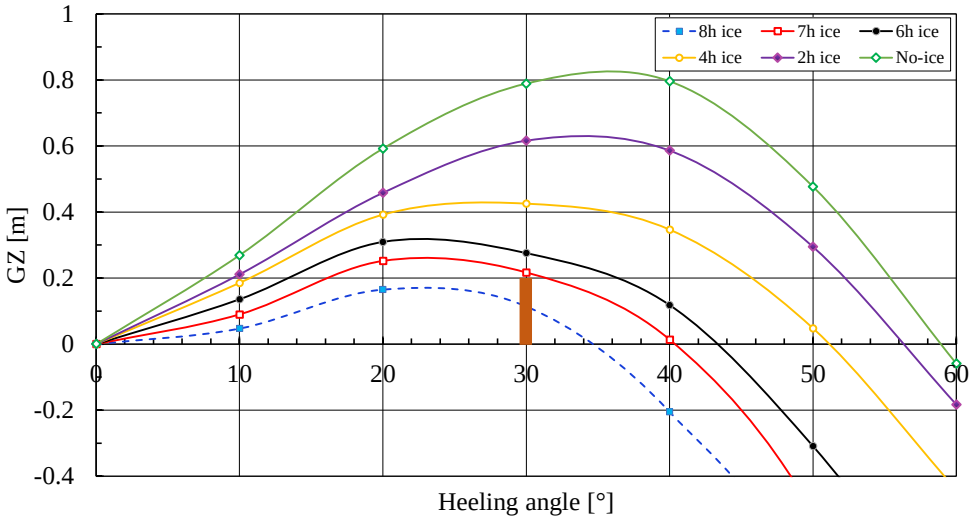

Fig. 5 GZ curves for both the No-ice and 6h ice conditions.

Fig. 5 revealed that the presence of ice significantly reduces the GZ values of the polar ship. When the duration

of ice accumulation reaches 6 hours, as an example, the angle at which the peak restoring arm occurs shifts from 30–40 degrees to approximately 20 degrees, whereas the peak value decreases from 0.80 m to 0.31 m. Furthermore, the angle of vanishing stability changes from 58.68 degrees to 42.88 degrees. This decline indicates that the ship is more prone to losing stability when heeled, consequently increasing the risk of capsizing; these factors can have a coupled impact on the stability of the polar ship. Although ice accumulation accounts for only 9.15% of the polar ship displacement, its positioning on the freeboard, deck, and superstructure substantially elevates the center of gravity. With the continuous accumulation of ice, the peak value of the GZ curve progressively decreases. Between 7 to 8 hours of icing, the safety limits specified by the IMO IS Code—including requirements for the GZ peak value and the area under the curve—are exceeded. This indicates that the loss of static stability due to ice accumulation has reached an unacceptable level for this polar ship. Consequently, the ice accumulation has a significant effect on the static stability of the polar ship.

Severe rolling may cause ship capsizing, which is a severe safety incident where a ship exceeds the safe limits of the roll angle, leading to an inability to restore balance and ultimately resulting in ship sinking. This issue has been a major focus in the maritime and offshore engineering fields for many years. The current specifications set requirements through stability standards such as the angle of vanishing stability and the righting lever. The static stability analysis clearly demonstrated that the polar ship with 6-7 hours of ice accumulation can still maintain adequate static stability in typical high-risk icing environments. Evaluating the impact of icing on polar ship stability solely on the basis of the righting lever and angle of vanishing stability may lead to an overestimation of roll stability, resulting in overly optimistic conclusions. Therefore, employing a more comprehensive loss-of-dynamical-stability assessment method that utilizes roll motion response, rather than relying solely on static stability assessments, is crucial for ensuring the navigational safety of polar ships.

3.2 Mathematical model of roll motion

To assess the stability of ice-affected ships in waves, accurately solving the response of ships to roll motion is essential. In this study, the roll motion of a polar ship under dead ship condition with and without ice accumulation under the combined action of wind and waves is considered. Under the influence of ice accumulation, the draft and center of gravity of the polar ship are altered, leading to changes in the damping force, restoring force, and inertial force. The impact of ice on these parameters results in a coupling effect on the roll motion response of the polar ship. A single-degree-of-freedom (SDOF) model of dead ship transverse rolling motion is established to calculate

the transverse motion response of both intact and ice-covered ships. The time-domain equation of motion for transverse rolling in a nonperiodic irregular wave for a dead ship is as follows (Bulian, 2004):

$$(I_{44} + A_{44}) \cdot \ddot{\varphi}(t) + B_{44} \cdot \dot{\varphi}(t) + B_{44\mathrm{n}} \cdot \dot{\varphi}^3(t) + \Delta \cdot GZ(\varphi(t)) = M_{wave}(t) + M_{wind}(t) \tag{10}$$

where I_{44} represents the roll moment of inertia of the ship, A_{44} represents the additional roll moment of inertia of the ship, φ_t denotes the roll angle at time *t*, $\dot{\varphi}_t$ represents the roll angular velocity at time *t*, $\ddot{\varphi}_t$ represents the roll angular acceleration at time *t*, B_{44} and B_{44n} are linear and nonlinear roll damping terms, $M_{wave}(t)$ represents the random irregular wave-induced moment that uses the superposition of 2000 wave components, and $M_{wind}(t)$ represents the wind heeling moment, including steady wind and gusts.

In the SDOF model, restoring the perturbation moment is a classic simplified method for calculating the wave moment. This is because the restoring perturbation moment is much larger than the damping perturbation moment and the inertia perturbation moment components in the wave moment. Therefore, the formula for the wave moment is given as follows:

$$M_{wave}(t) = \Delta \cdot GM \cdot \gamma(\omega_n) \cdot \zeta(t) \tag{11}$$

where $\gamma(\omega_n)$ is the effective wave slope coefficient, with a value of 0.847 in this paper, which is calculated via an empirical formula (Faltinsen O M, 1993), and where ζ_t is the waveform function calculated via linear superposition:

$$\zeta(t) = \sum_{n=1}^{N_w} k_w \cdot \xi_{An} \cdot cos(\omega_n t + \varepsilon_n) \tag{12}$$

$$\zeta_{An} = \sqrt{2S(\omega_n)\delta\omega} \tag{13}$$

where N_w is the number of irregular waves; k_w is the wavenumber; ξ_{An} is the wave amplitude for regular waves; ω_n is the wave frequency; and ε_n is the random phase angle. $S(\omega_n)$ represents the wave spectrum, with the ITTC two-parameter spectrum being selected for this study. Its general form is given by:

$$S(\omega_n) = \frac{173\overline{\zeta_{W/3}^2}}{T_1^4\omega^5}\exp\left(-\frac{691}{T_1^4\omega^4}\right) \tag{14}$$

The effect of wind on a ship is primarily exerted through wind pressure, which generates forces and moments that influence the ship's behavior. Wind loads have a significant effect on structures with high centers of gravity and large windward areas. In polar regions, the risk of severe winds cannot be overlooked, making wind loads an important environmental load in the single-degree-of-freedom capsizing model of polar ships.

The wind moment includes the effects of steady wind and unsteady wind. Steady winds act continuously on the ship without variation over time, causing a constant heeling angle. The expression for the wind moment due to steady wind is given as follows:

$$\bar{M}_{wind} = 0.5 \cdot \rho_{air} \bar{V}_w{}^2 A_L C_y (H_w + H_{yd}) \tag{15}$$

where ρ_{air} is the air density, which is 1.229 kg/m^3. A_L is the lateral wind-exposed area of the ship. C_y is the wind moment coefficient and references the data range 0.5 to 1.2 from the Blendermann database (1994). Considering the large superstructure area of the polar ship analyzed in this study, a higher value of C_y = 1.0 was chosen. CFD simulations were conducted to calculate the wind moment, yielding a validation result of 1.002, and the impact of minor differences in the wind moment coefficients on the roll motion response of the ship can be considered negligible. H_w and H_{yd} are the vertical distances from the waterline plane to the wind field center of action and the wave force center of action, respectively. $\overline{V_w}$ is the steady wind speed, which can be evaluated on the basis of the significant wave height due to the interaction between the wind and waves:

$$\overline{V_w} = \left(\frac{H_S}{0.06717}\right)^{2/3} \tag{16}$$

Unsteady wind, also known as gust wind, varies with time when acting on a ship. The Davenport gust spectrum is used to simulate the effects of gust wind in this work, and the expression is as follows:

$$S_v(\omega) = 4K \cdot \frac{\overline{V_w}^2}{\omega} \cdot \frac{X_D{}^2}{(1 + X_D{}^2)^{\frac{4}{3}}} \tag{17}$$

where K is a constant with a value of 0.003.

$$X_D = 600 \cdot \frac{\omega}{\pi \overline{V_w}} \tag{18}$$

Therefore, the wind moment due to the combined effects of steady wind and gusty wind is given as follows:

$$M_{wind}(t) = 0.5 \cdot \rho_{air} (\overline{V_w} + V_g(t))^2 A_L C_y (H_w + H_{yd}) \tag{19}$$

where $V_g(t)$ is the gusting wind speed, and its expression is given as:

$$V_g(t) = \sum_{n=1}^{N_w} \sqrt{2 S_v(\omega_n) \delta\omega} \cdot \cos(\omega_n t + \varepsilon_n) \tag{20}$$

3.3 Roll-damping term

The roll damping coefficient is a critical parameter that describes the damping characteristics of a ship's roll motion under external lateral forces. The primary experimental techniques for estimating roll damping include roll decay, forced roll, and excited roll tests (ITTC, 2017). Roll decay testing is the most commonly used technique and involves the measurement of roll decay motion in calm water. While relatively straightforward to conduct, this test requires a scaled model of the ship. As an alternative to physical model experiments, CFD techniques can be applied.

Several studies have utilized 3D CFD simulations (Adrian Lungu, 2020; Chao Chen et al., 2023). To assess the vulnerability of dead ships, the IMO recommends the use of simplified Ikeda's method to estimate the transverse damping coefficient for calculation purposes. However, there may be significant discrepancies between the estimated transverse damping coefficient obtained via Ikeda's method and the actual values. To improve the accuracy of calculating the transverse damping coefficient, this study employs CFD to simulate the free decay motion of the ship during transverse rolling.

3.3.1 CFD method

In the CFD method, fluid motion can be mathematically described via a system of partial differential equations, following the principles of mass, momentum, and energy conservation per unit volume of fluid. The continuity and momentum equations for incompressible fluids are typically expressed via tensor notation, as described by Ferziger et al. (Ferziger et al., 2019).

$$\frac{\partial(\rho\bar{u}_i)}{\partial x_i} = 0 \tag{21}$$

$$\frac{\partial(\rho\bar{u}_i)}{\partial t} + \frac{\partial}{\partial x_i}\left(\rho\overline{u_i u_j} + \rho\overline{u_i' u_j'}\right) = -\frac{\partial\bar{p}}{\partial x_i} + \frac{\partial\bar{\tau}_{ij}}{\partial x_j} \tag{22}$$

$$\bar{\tau}_{ij} = \left(\frac{\partial\bar{u}_i}{\partial x_j} + \frac{\partial\bar{u}_j}{\partial x_i}\right)/v \tag{23}$$

where $\bar{u_i}$ and $\bar{u_j}$ are the average velocity vectors of flow (i, j = 1, 2, 3); x_i are the Cartesian coordinates; $\bar{p}$ is the mean pressure; ρ is the fluid density; $\overline{u_i' u_j'}$ is the negative value of the Reynolds stresses; $\overline{\tau_{ij}}$ are the mean viscous stress tensor components; and v is the coefficient of fluid viscosity.

The Reynolds stress can be simulated as a function of the average flow rate via the concept of turbulent eddy viscosity. The most commonly used method is the Boussinesq approximation:

$$\rho\overline{u_i u_j} = -u_t\left(\frac{\partial\bar{u}_i}{\partial x_j} + \frac{\partial\bar{u}_j}{\partial x_i}\right) + \frac{2}{3}\left(\rho\cdot ke + u_t\frac{\partial\bar{u}_{ke}}{\partial x_{ke}}\right)\delta_{ij} \tag{24}$$

where u_t represents the turbulent eddy viscosity, ke and δ_{ij} represent the turbulent kinetic energy and Kronecker delta, respectively.

Through CFD numerical simulations of free roll decay, the time history of the transverse rolling motion is obtained, from which the decay curve is plotted. The transverse damping coefficient of a ship, which significantly impacts its transverse rolling motion, is determined by plotting this decay curve via the simulated transverse roll amplitude for analysis. The decay relationship of the decay curve is as follows:

$$\Delta\varphi_A = a_r\varphi_{Am} + b_r{\varphi_{Am}}^2 \tag{25}$$

In the above equation, a_r represents the linear decay coefficient, b_r represents the nonlinear decay

coefficient, $\Delta\varphi_A$ represents the difference between the amplitudes of two consecutive half-cycles, and φ_{Am} represents the average value of adjacent amplitude values.

According to the energy relationship, the decay curve reflects the damping characteristics of the rolling motion. Therefore, in the mathematical model of polar ship rolling motion, the damping force coefficients B_{44} and B_{44n} can be calculated via the coefficients a and b obtained from fitting the decay curve:

$$B_{44} = -\frac{4(I_{44}+A_{44})}{\mathrm{T_r}} \cdot a_r \tag{26}$$

$$B_{44\mathrm{n}} = -\frac{3(I_{44}+A_{44})}{4} \cdot b_r \tag{27}$$

where T_r is the natural period of polar ship roll motion.

Within the framework of CFD simulations, the scale ratio of the polar ship is 1:60, effectively reducing the computation time and avoiding the significant computational resource consumption required for free-decay numerical simulations using real ship scales. Previous research on the scale effects between model-scale ships and full-scale ships has indicated that the influence of free-decay experiments conducted to obtain dimensionless natural periods and damping coefficients for roll motion is negligible and can be disregarded (Yang et al., 2018). Consequently, the damping coefficient obtained through CFD computations at the model scale can be employed in subsequent studies. The parameters of the model are shown in Table 3.

3.3.2 Free decay simulation

The key to turbulent flow calculations is to determine u_t, and several numerical models have been proposed for this purpose. In this study, the widely used and implementable standard k-ε model is adopted, which provides a good compromise between robustness, computational cost, and accuracy. Numerical calculations are carried out via the finite volume method. A second-order upwind scheme is employed to solve the transient, convection, and diffusion terms, and a second-order time discretization is implemented in the time domain solution. The iterative calculations are performed via the semi-implicit method for pressure-linked equations (SIM SIMPLE) algorithm. The time step is 0.005 seconds.

To ensure the accuracy of the numerical simulations, this study adopts a validated numerical decay scheme based on experimental data (Chai et al., 2024). In this approach, overlapping grid technology is employed, with densified grids set around the hull and a free liquid surface to capture flow details more accurately. The number of grid nodes theoretically has a direct effect on the accuracy of the computational results. Therefore, on the basis of established numerical decay simulations, the grid independence of the polar ship's numerical decay simulation is

verified. Four grid schemes are designed, differing in total node count due to varying base grid sizes and densified grid designs. The parameters of each grid scheme are shown in Table 4. Fig. 6 shows the grids of Grid scheme 3, including the background grid, overlapping grid, and densified grid.

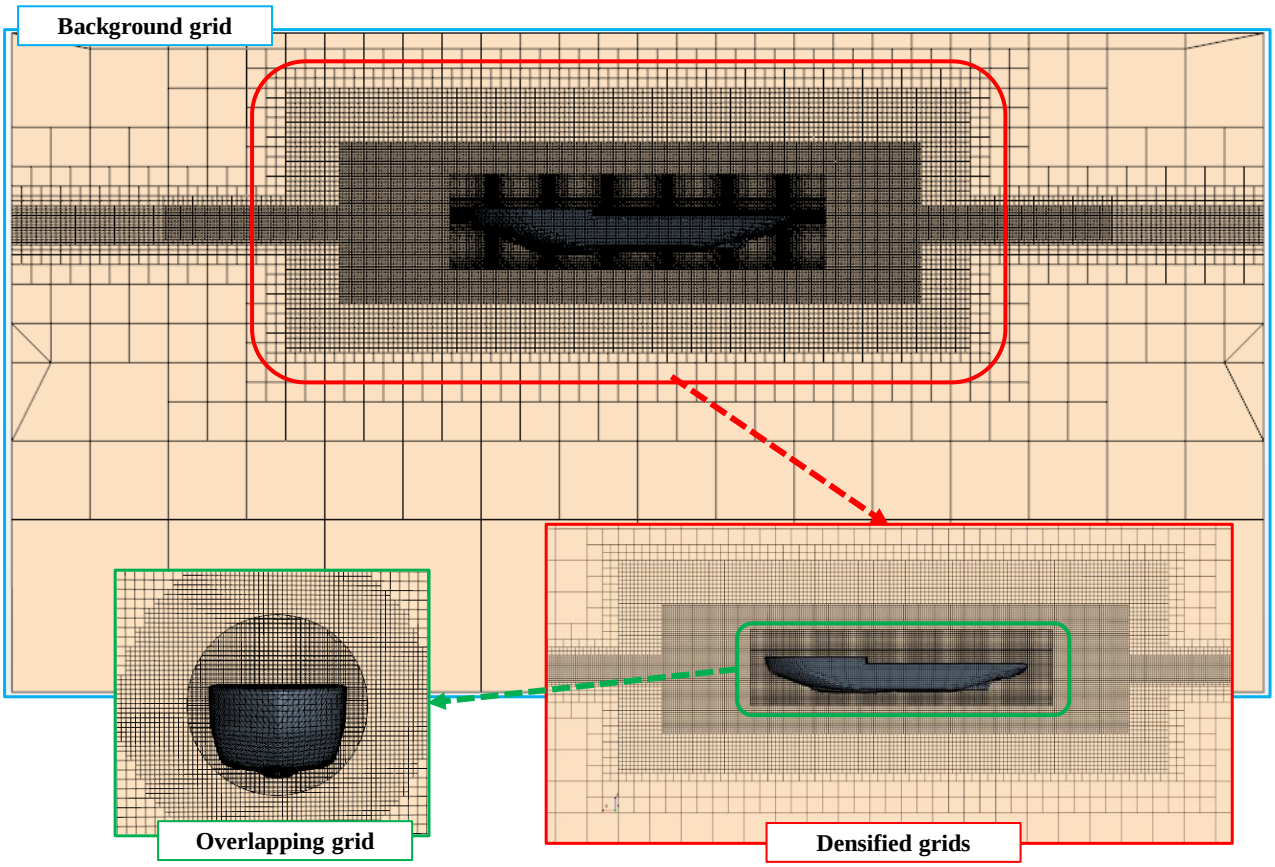

Fig. 6 The grids of Grid Scheme 3 include a background grid, an overlapping grid, and densified grids.

Table 4 The parameters of different grid schemes.

Grid scheme	Basic dimensions(m)	Amount of the grid
Grid 1	1.5	$1.09*10^6$
Grid 2	1.2	$1.95*10^6$
Grid 2	1.0	$2.86*10^6$
Grid 4	0.8	$4.69*10^6$

Upon commencing the numerical simulation of free decay, the ship model initiates rolling owing to its initial heel angle. Analysis of the cloud map depicting free surface waves reveals that as free decay advances, concentric waves emanate from the ship model and attenuate toward the computational domain boundaries, as depicted in Fig. 7.

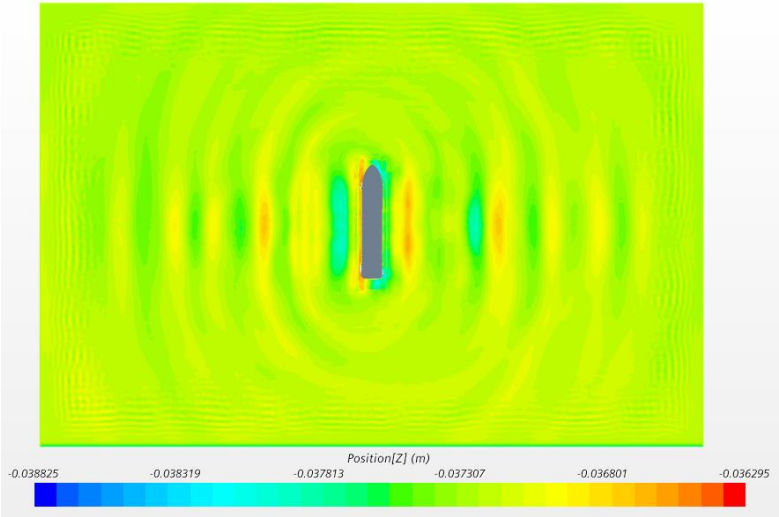

Fig. 7 Wave height distribution cloud map of the free liquid surface of free decay.

A comparison of the free decay time history curves of the polar ship without ice accumulation under different grid schemes is shown in Fig. 8. The stress–strain curves for mesh schemes 3 and 4 closely approximate each other, whereas those for schemes 1 and 2 exhibit substantial deviations, suggesting that errors result from inadequate mesh density. During grid independence verification, ensuring computational accuracy while also balancing computational costs and precision is crucial. Therefore, grid scheme 3 is ultimately chosen as the grid scheme used for the free decay numerical simulation in this study. Grid validation confirms that the CFD-based numerical model accurately simulates free decay-induced rolling, facilitating the calculation of roll damping coefficients for the SDOF model under both icy and ice-free conditions.

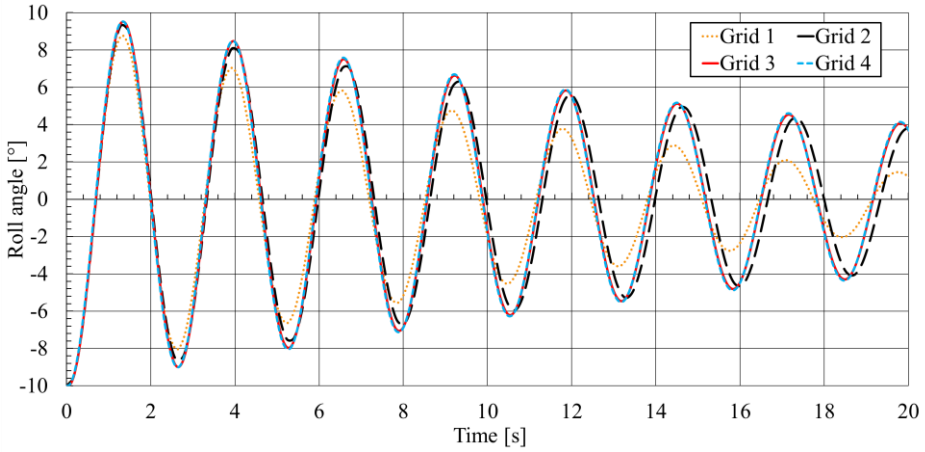

Fig. 8 Free decay time history curves under different grid schemes.

In this work, the decay curve is calculated via numerical simulation via the CFD method for free-decay motion. The coefficients *a* and *b* are then determined for the No-ice and 6h ice conditions. An initial inclination angle of 20°

is selected in the calculation to conform to the nonlinear characteristics of motion in waves. The curves of extinction and fitted values under both No-ice and 6h ice conditions for the polar ship are shown in Fig. 9.

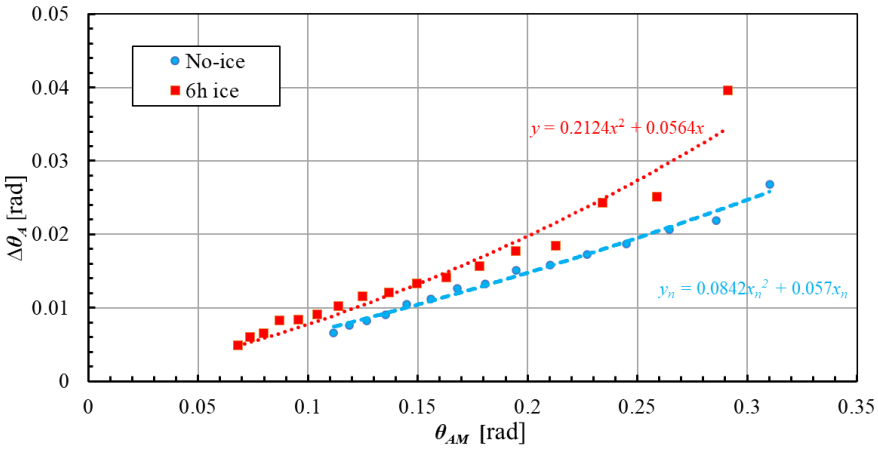

Fig. 9 Curves for roll damping and fitted values under both 6h ice and No-ice conditions.

Under No-ice condition, a_r = 0.0570 and b_r = 0.0842, whereas under the 6h ice condition, a_r = 0.0564 and b_r = 0.2124. Fig. 9 reported that ice accumulation has a significant effect on the roll damping term, with both linear and nonlinear damping varying to a certain extent. In terms of the elimination coefficient, the linear coefficient a_r under the 6h ice condition decreased by 1.05%, whereas the nonlinear coefficient b_r increased by 152.26% compared with that under the no-ice condition. This phenomenon arises from the increase in displacement caused by ice buildup, resulting in increased inertia. The increased volume and cross-sectional area of the submerged portion led to greater viscous damping and additional mass, which ultimately contributed to the increase in roll damping.

3.4 Dynamical analysis of roll motion with ice accumulation

After completing the calculations for roll damping, restoring force, wave moment, and wind moment, a single-degree-of-freedom roll motion model of the dead ship in crosswinds and crosswaves is developed for the polar ship. For the 6h ice accumulation and No-ice conditions, the model is adjusted on the basis of calculations of static stability. The changes due to ice accumulation in weight, the center of gravity, the moment of inertia, roll damping, and the restoring force are considered. The polar ship conducted roll motion response calculations under hazardous sea conditions.

To align with the meteorological and hydrological conditions used for forecasting ice accumulation, we selected a wind speed of V_w=20.6 m/s and a wave height of H_s=5.5 m for the transverse rolling motion response

calculations of the polar ship under both No-ice and 6h ice conditions. On the basis of relevant studies of wave distributions in polar regions, an irregular wave is generated with a frequently observed zero-crossing period of T_z=14 s. These environmental parameters are consistent with those used in the ice accumulation calculations in Section 2.2. A 3600-second continuous simulation is conducted for both No-ice and 6h ice conditions, with the results shown in Fig. 10.

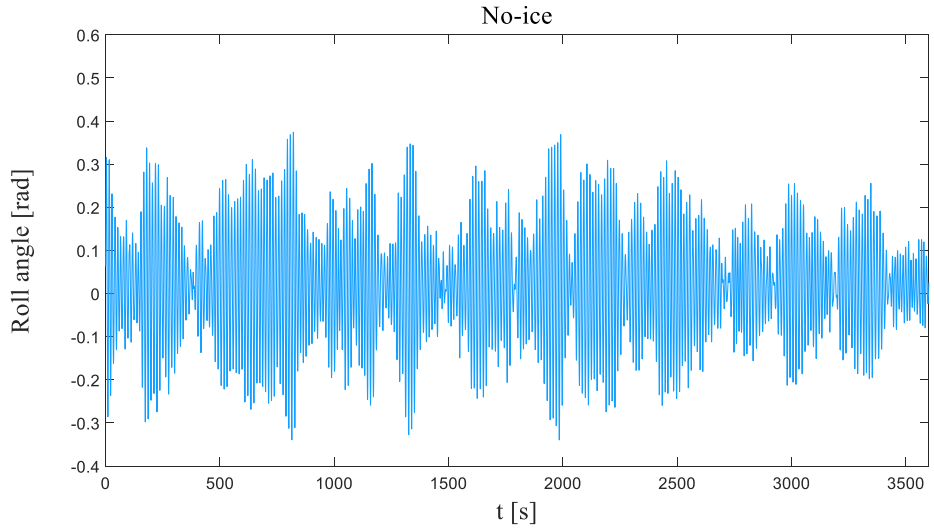

(a) No-ice

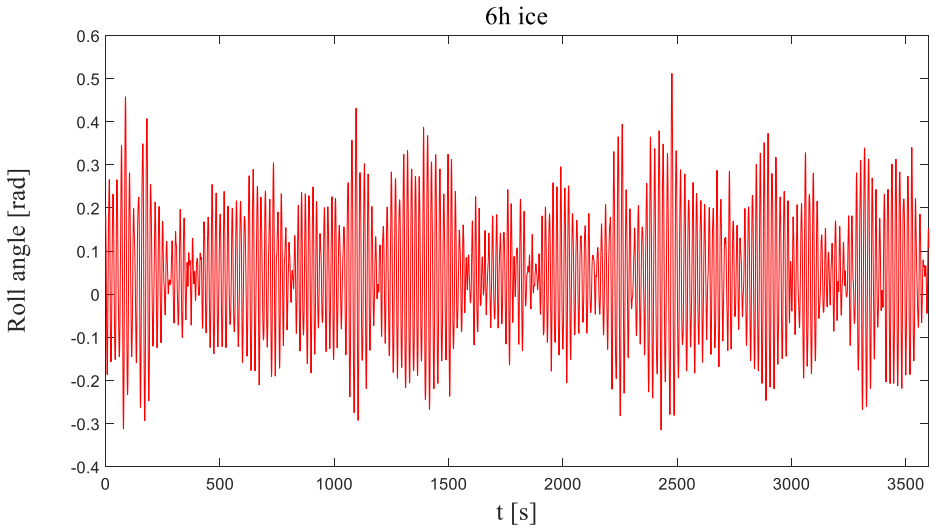

(b) 6h ice

Fig. 10 Roll motion response time history under No-ice and 6h ice conditions.

The time history of the roll angle reflects only the variation in roll motion over time, providing limited information because of the influence of random waves. As a result, the analysis in the time domain is relatively constrained. To gain a more comprehensive understanding of the impact of ice accumulation on the ship's roll

motion, frequency domain analysis, which reveals the dominant frequency components of the roll motion and their amplitude distributions, is more effective. Therefore, the roll motion response spectra of the polar ship under both No-ice and 6h ice conditions are computed, as illustrated in Fig. 11.

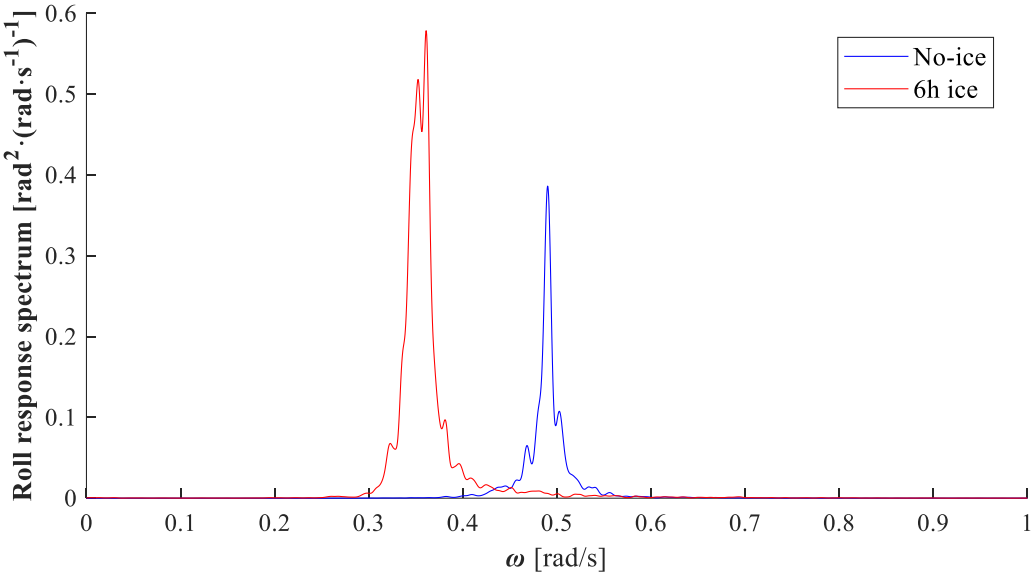

Fig. 11 Spectrum of roll motion for the polar ship under No-ice and 6h ice conditions.

Fig. 11 clearly shows that the average and maximum roll amplitudes of the polar ship under the 6h ice condition are significantly greater than those under the no-ice condition. This demonstrates the coupled effects of changes in parameters such as displacement, center of gravity, moment of inertia, righting lever, and initial stability on roll motion responses due to ice accumulation. From the energy spectra shown in Fig. 11, it is evident that the value of the roll motion response energy spectrum of the polar ship under 6h ice condition is greater than that under No-ice condition, and the significant ice accumulation leads to a noticeable alteration in the natural roll period of the polar ship. This significant disparity highlights the substantial impact of ice accumulation on the dynamic stability of the polar ship under the action of wind and waves and under extreme environmental conditions.

The response of the polar ship roll motion in irregular waves with different T_z and H_s values under both No-ice and 6h ice conditions are illustrated in Fig. 12. To minimize the influence of randomness, the comparative values were defined as the maximum roll angles obtained from 50 simulations, each lasting 3600 seconds. For each period, 50 sets of 3600-second calculations were performed, and the maximum roll angles from these 50 sets were computed to show the impact of T_z and H_s on ice accumulation.

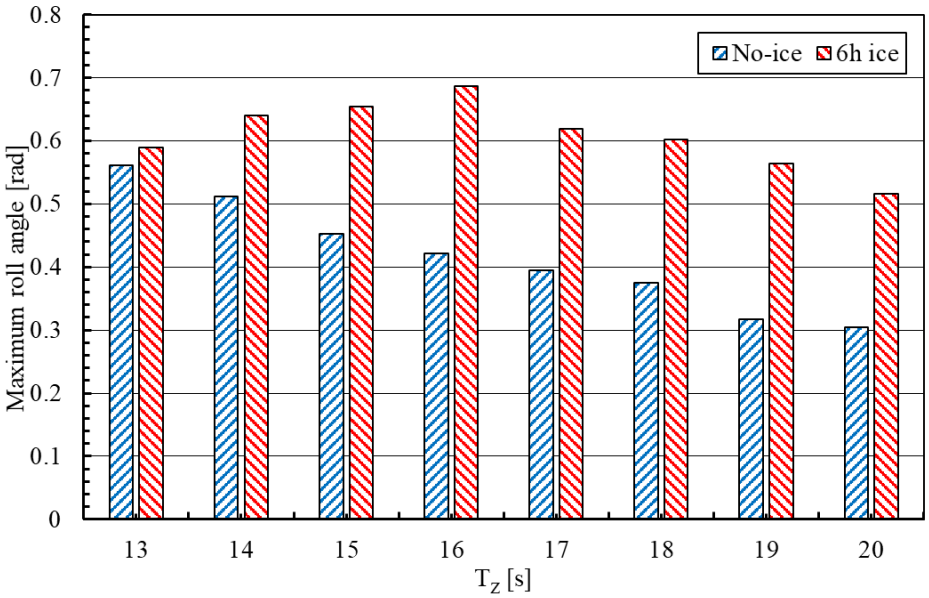

(a) Different T_z, H_s = 5.5 m

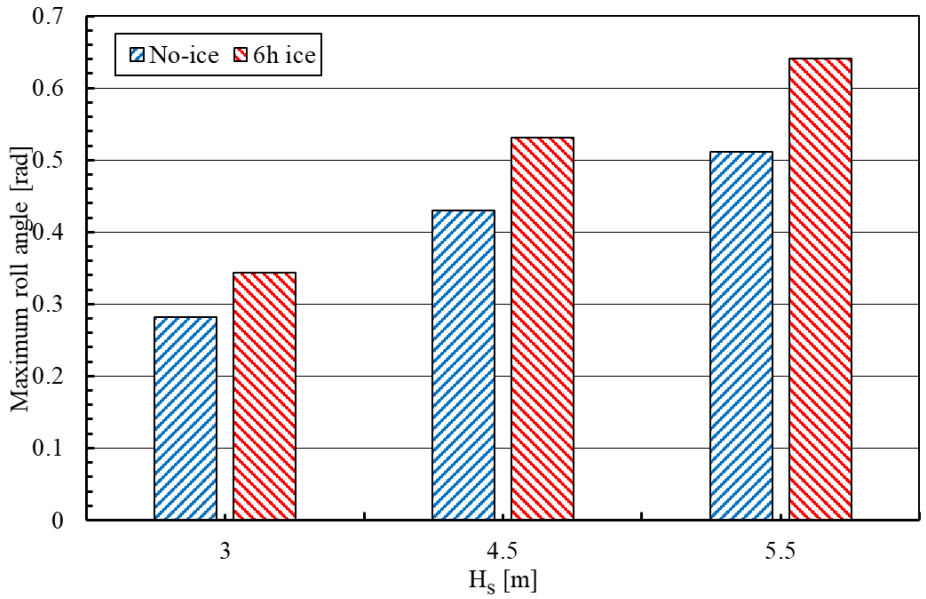

(b) Different H_s, T_z = 14 s

Fig. 12 Roll motion response to irregular waves with different T_z and H_s values under both No-ice and 6h ice conditions

Fig. 12 (a) shows that, compared with the No-ice condition, the polar ship with 6h ice accumulation has a significantly larger roll motion response under different H_s values due to the occurrence of ice accretion. Notably, the increased ice weight altered the ship's natural period, shifting it to approximately 16 s under the 6h ice condition. Fig. 12 (b) illustrates the influence of varying H_s on the roll motion of the polar ship. As the wave height increases, the roll motion response of the polar ship intensifies, with the roll under the 6h ice condition consistently exceeding

that of the No-ice condition at the same wave height.

Notably, the roll angle under the 6h ice condition reached a maximum of 29.31°, which does not exceed the stability loss angle of 41.54° indicated by the GZ curve. The 3600-second roll motion response calculations show that the 6h ice condition still meets the safety requirements for navigation and has a large safety margin. However, this assessment overlooks the complexity and randomness of polar marine environments. Relying solely on roll motion response analysis or GZ curve requirements is insufficient to capture the potential hazards that polar vessels may face under icy conditions. In dynamic stability evaluations, the results of single or multiple motion response calculations may fall within acceptable ranges but fail to reflect the potential extreme roll motion values that polar ships could encounter under ice accumulation conditions. This approach does not provide an indication of whether the design limits may be exceeded in the most unfavorable scenarios. Therefore, this study employs an extreme value forecasting method based on the ACER theory to conduct a more comprehensive and quantitative evaluation of the dynamic stability of polar ships under ice accretion conditions.

4 Extreme value analysis

To assess the impact of ice accumulation on the stability of the polar ship accurately, this study employs extreme value prediction methods to forecast the extreme values of roll motion responses under the No-ice and 6h ice conditions. Extreme value forecasting is a method used to predict the potential extreme response values of a system in the future. It relies on system dynamics models, statistical data, or numerical simulations as inputs to estimate the maximum or minimum values of response variables over a specified period or under certain conditions. This approach allows for the quantification and effective prediction of potential hazards associated with ice conditions. On the basis of Section 3.4 Dynamical analysis of roll motion with ice accumulation, 50 simulations are conducted on the roll motion of a polar ship in dead ship conditions under crosswind and crosswave conditions, with each simulation lasting 3600 seconds. The roll motion response φ of 50 groups was utilized as input, and the possible extreme values were predicted via the ACER method.

4.1 ACER method

The ACER method is a numerical approach that effectively handles non-stationary datasets and leverages all available data in the process of extreme value prediction; it works by analyzing the tail behavior of the response distribution, focuses on the asymptotic constant that characterizes the extreme values over time, and has excellent

performance in predicting the corresponding movements in the fields of ships and ocean engineering. η represents the extrema of φ, and the cumulative distribution $P(\eta)$ of η can be expressed as follows:

$$P(\eta) \approx exp(-(Q-k+1)\cdot \mathrm{ACER}_k(\eta)) \approx exp(-(Q-k+1)\cdot \hat{\varepsilon}_k(\eta)) \tag{28}$$

In the above formula, Q represents the number of peak values of roll motion within 50 hours. Where $\mathrm{ACER}_k(\eta)$ is the ACER function; $\hat{\varepsilon}_k(\eta)$ represents the empirically estimated ACER function of order k on the basis of the data derived from 3600 s data of φ within the roll motion time history of the 50 sets.

To satisfy the requirements of exceedance probability computation, k denotes the order of the ACER function, $k \ll Q$, and constructing the sequence of ACER functions of different orders k forms a core aspect of the ACER method. Fig. 13 illustrates the extraction of local peak values for different k when $\eta = 0.2$ as an example. For $\varepsilon_k(\eta)$, any group of consecutive exceedances separated by $(k-1)$ non-exceedances is considered a clump. In Fig. 13, when $k = 2$, there are 4 clumps, whereas the number of clumps decreases to 3 when $k = 3$. The average number of exceedance clumps under different conditions decreases as the conditions (separation requirements) become more stringent, which facilitates the study of extreme behaviors in the response process, particularly the clustering effect of peak values. Increasing the order k can effectively improve the accuracy of the equation and enhance the convergence of the ACER function, but it also reduces the utilization of data for extreme value prediction. Therefore, the value of k should be kept as small as possible under the condition of a negligible difference in accuracy.

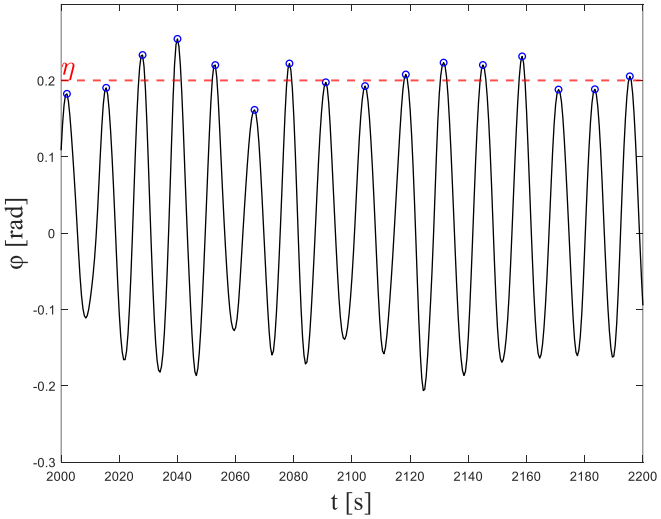

Fig. 13 The extraction of local peak values for different k when $\eta = 0.2$

Research in the field of ship motion response via the ACER method has shown that the ACER functions $\hat{\varepsilon}_k(\eta)$ corresponding to different extreme responses exhibit high regularity, especially in the tail region $\eta > \eta_0$,

which is very close to $exp\{-a-(\eta-b)^c\}$. Here, a, b, and c are constants, and $b \le \eta_0$, $a > 0$, and $c > 0$. Thus, the empirical ACER function is assumed to have the following structure:

$$\hat{\varepsilon}_k(\eta) \approx q_k \, exp\{-a_k(\eta-b_k)^{c_k}\}, \eta \ge \eta_0 \tag{29}$$

In the formula above, a_k, b_k, c_k and q_k are constants related to the order k and are also influenced by the collected data. The values of these constants can be determined through optimization fitting at different levels via the mean square error function:

$$F(q_k, a_k, b_k, c_k) = \sum_{i=1}^{M} \rho_i \left|\ln \hat{\varepsilon}_k(\eta_i) - \ln q_k + a_k(\eta_i - b_k)^{c_k}\right|^2 \tag{30}$$

In the above formula, η_i represents the estimated extreme level of the empirical ACER function, whereas ρ_i is a weight factor that assigns higher weights to reliable data points. Typically, there is a negative correlation between two variables. The value of ρ_i can be obtained via the 95% confidence interval of the empirical ACER function:

$$CI^{\pm}(\eta_i) = \hat{\varepsilon}_k(\eta_i) \cdot \left(1 \pm \frac{1.96}{\sqrt{(Q-k+1)\hat{\varepsilon}_k(\eta_i)}}\right) \tag{31}$$

In summary, the application of the ACER method in extreme value prediction is achieved by representing the extreme distribution through the average conditional exceedance rate of different orders *k*. The empirical tail region of extreme values can be captured with high accuracy by fitting a parametric function to the extreme distribution. Due to space limitations, only a brief introduction to the ACER method is provided here. For a more detailed explanation of the principles and development of the ACER method for extreme value estimation, readers are referred to Naess et al. (2024).

4.2 Extreme value analysis of the roll response

To assess the navigation safety of the polar ship, a total of 50 sets of single 3600-second simulations are conducted for the polar ship under both No-ice and 6h ice conditions. The meteorological and hydrological environmental parameters were consistently set as follows: T_z = 14 s, H_s =5.5 m, and V_w = 20.6 m/s. On the basis of these simulations, extreme value prediction studies are conducted via the ACER method.

To forecast the extreme roll motion responses of the polar ship under No-ice and 6h ice conditions using the ACER method, constructing and selecting ACER functions of various orders is essential. This process balances data utilization with the accuracy and convergence of the ACER functions. The empirical ACER functions for roll motion responses under the No-ice and 6h ice conditions are illustrated in Fig. 14.

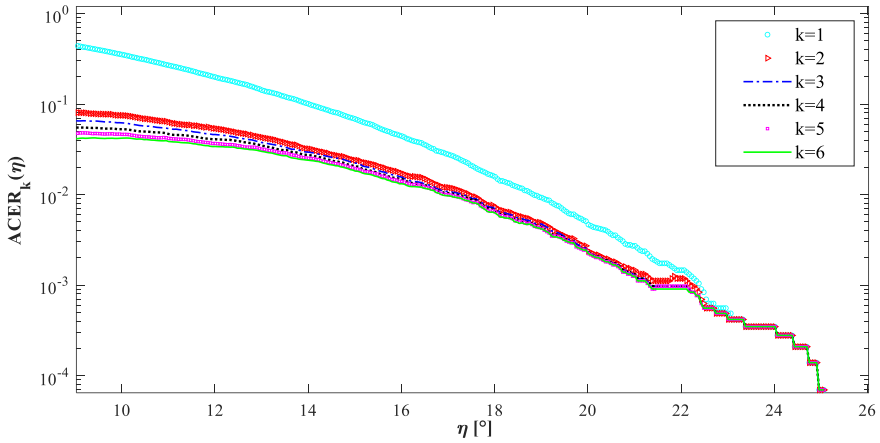

(a) No-ice

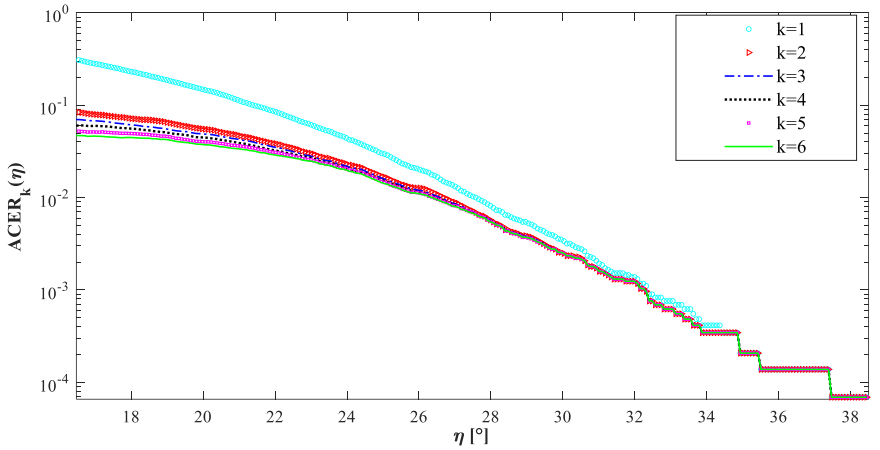

(b) 6h ice

Fig. 14 Empirical ACER functions for roll motion responses under No-ice and 6h ice conditions.

Comparative analysis of empirical ACER functions of different orders reveals that a second-order function accurately represents the roll motion responses for the No-ice and 6h ice conditions considered in this study. While offering improved convergence, higher-order empirical ACER functions do not significantly differ from the second-order function and require the exclusion of more data points. Given the trade-off between data retention and convergence, the second-order empirical ACER function is chosen for the extreme value prediction.

After the order of the empirical ACER function is determined, the corresponding functions are constructed, and the extreme value prediction results with exceedance probability $\lambda = 0.01$ are presented in Fig. 15.

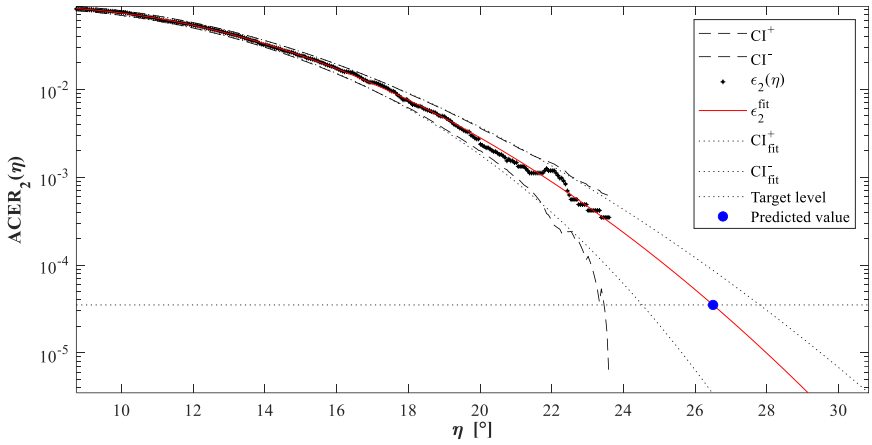

(a) No-ice

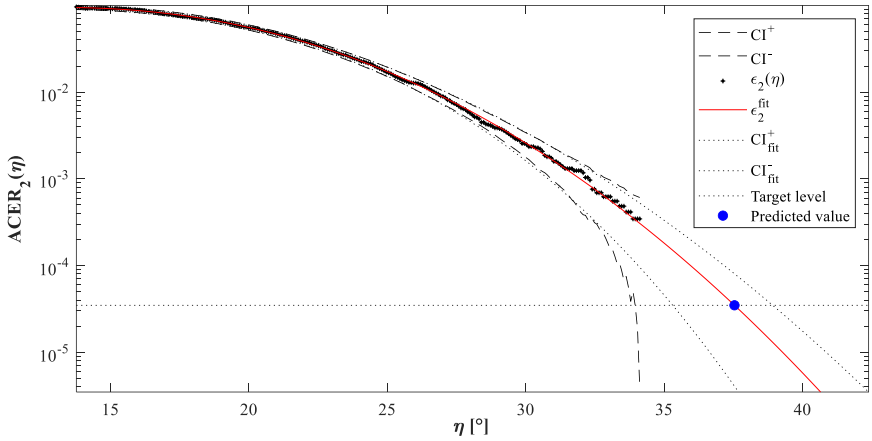

(b) 6h ice

Fig. 15 Extreme value prediction results under No-ice and 6h ice conditions.

Fig. 15 shows that for an exceedance probability of $\lambda = 0.01$, the extreme roll motion response of the polar ship under No-ice condition is 26.50°, whereas under 6h ice condition, it is 37.54°. The ACER method predicts a 41.66% difference in extreme values, indicating that the effect of ice accumulation on roll motion stability is more pronounced and requires greater attention. Obviously, extreme values of the roll motion response under ice condition exceed those under No-ice condition, and the extreme value prediction analysis further quantifies the hazards posed by ice accumulation to the polar ship.

Notably, the extreme values of the roll motion response for the polar ship under 6h ice condition increased by 41.66% compared with that under No-ice condition with H_s = 5.5 m and T_z=14 s. Although the forecasted extreme roll angle value of 37.54° remains below the critical stability angle of 42.88° after icing, it already approaches this threshold, and the risk of capsizing exists if the maximum roll angle exceeds the safety limit. Considering the complexities of marine environmental factors, the actual risk of capsizing may be even greater. Therefore, it is

crucial to accurately quantify and design safety margins for ice stability in polar regions on the basis of extreme prediction theory and the ACER method and to pay heightened attention to the substantial risks posed by ice during navigation.

To assess the reliability of the ACER method for forecasting extreme roll motion responses of a polar ship under icing conditions, a comparison is made with the classic Monte Carlo method. The Monte Carlo method is a numerical technique used to solve complex problems through random sampling and probabilistic simulation. In this study, the method is applied to calculate threshold values at different probabilities on the basis of 50 sets of roll motion response data. For more details on the related theory, refer to the literature (Xu S, 2021). A comparison of the two methods is shown in Fig. 16.

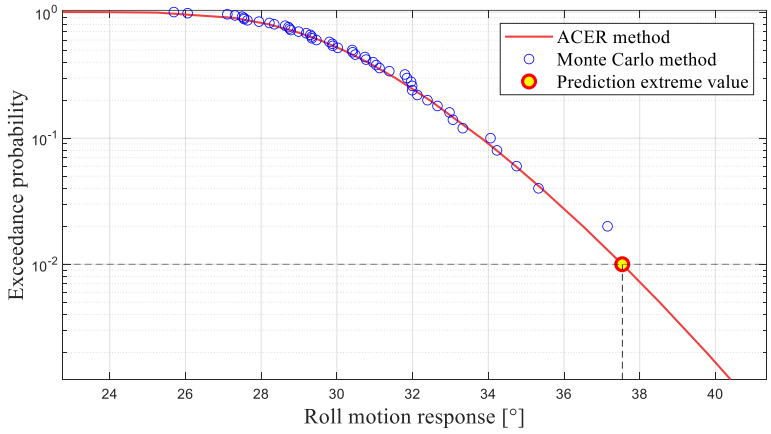

Fig. 16 Comparison of the ACER method and Monte Carlo method for extreme value prediction of roll motion response under 6 h ice conditions

The comparison between the ACER method and the Monte Carlo method for predicting extreme roll motion values of the polar ship under 6h ice condition demonstrates that, under icing condition, both the ACER method and the Monte Carlo method demonstrate good applicability, providing effective forecast data to assist in assessing the stability risk posed by icing for polar ships. The ACER method constructs ACER functions of varying orders for extreme value prediction. This method is also applicable to non-stationary datasets and utilizes all amplitude data for forecasting, which helps avoid overly stringent design requirements. Employing the ACER method for assessing the stability of polar ships with ice accumulation provides a more accurate quantification of extreme roll angles under hazardous sea conditions, aiding in polar ship design.

5 Conclusions

This study examines the impact of ice accumulation on the static and dynamic stability of a polar ship in typical wind and wave environments in the Arctic region. A simplified method for calculating the amount of ice accumulation on polar ships is proposed. On this basis, the static stability loss of a polar ship under 6h ice conditions is calculated, and changes in the roll motion response are determined by constructing an SDOF ship motion model. Finally, the ACER method is utilized to further assess the impact of ice accumulation on the ultimate roll stability of the polar ship. Several conclusions can be drawn from this study:

1) The stability assessment of iced ships needs to account for variations in ice accumulation. By calculating the icing rate through the seawater spray volume and the thermodynamic processes of spray ice formation, combined with the definition of the hull icing area on the basis of relevant guidelines, a simplified icing rate prediction method is proposed. This enables the calculation of static stability for ships under different durations of icing.

2) Ice accumulation alters the initial stability height and the righting arm of polar ships. Under typical environmental conditions with 6 hours of icing, the peak value of the GZ curve for the polar ship decreases by 61.25%, and the angle of vanishing stability decreases by 36.85%. The boundary between 7 and 8 hours of icing is identified as the critical point where GZ no longer complies with the IS Code's static stability requirements.

3) The roll motion response of the polar ship with 6-hour ice accumulation is significantly higher than that under no-ice conditions in typical sea states. Ice accretion also alters the natural roll period and increases roll damping. Extreme value predictions based on the ACER method indicate a 41.66% increase in extreme roll values under 6-hour ice conditions at a probability level of $\lambda = 0.01$. This further highlights the loss of dynamic stability and the potential for extreme roll motions in polar ships with ice accretion.

This study advances the assessment of both static and dynamic stability for polar ships under icing conditions, laying a foundation for evaluating capsizing risk under extreme scenarios, defining safe operational boundaries, and optimizing route planning in polar navigation. Future work will explore the stability variations of polar ships with ice accretion under integrated environmental conditions, leveraging advanced ice prediction methods and multi-degree-of-freedom ship motion models to support the safe navigation of polar ships in Arctic regions.

Acknowledgments

This work is supported by the National Natural Science Foundation of China (NO.52201379). Supports from the Fundamental Research Funds for the Central Universities (WUT: 3120624109), State Key Laboratory of Structural Analysis, Optimization and CAE Software for Industrial Equipment, Dalian University of Technology

(GZ 231088) and Shanghai Key Laboratory of Naval Architecture Engineering (SE202305) are gratefully acknowledged.

References

Afzal M S, Kumar L, Chugh V, et al. Prediction of significant wave height using machine learning and its application to extreme wave analysis[J]. Journal of Earth System Science, 2023, 132(2): 51.

Ahmadi S, Aguilera A R, MacMillan B, et al. Studies of periodic seawater spray icing with unilateral NMR[J]. Journal of Magnetic Resonance, 2022, 334: 107109.

Blendermann W. Parameter identification of wind loads on ships[J]. Journal of Wind Engineering and Industrial Aerodynamics, 1994, 51(3): 339-351.

Bulian G, Francescutto A. A simplified modular approach for the prediction of the roll motion due to the combined action of wind and waves[J]. Proceedings of the Institution of Mechanical Engineers, Part M: Journal of Engineering for the Maritime Environment, 2004, 218(3): 189-212.

Chai W, Leira B J, Naess A. Probabilistic methods for estimation of the extreme value statistics of ship ice loads[J]. Cold regions science and technology, 2018, 146: 87-97.

Chai W, Qi J, Leira B J, et al. Extreme Value Analysis of Ship Roll Motion With Consideration of Ice Accumulation[C]//International Conference on Offshore Mechanics and Arctic Engineering. American Society of Mechanical Engineers, 2024, 87844: V006T07A003.

Chen C, Liu Y, Zhang W, et al. Free roll decay simulation of a polar research vessel with an anti-roll tank based on CFD[J]. Ocean Engineering, 2023, 285: 115429.

Dash A, Sahoo A K, Yadav A, et al. Computational modeling of freezing of water droplet impacting on an ice surface[J]. Materials Today: Proceedings, 2021, 41: 156-160.

Dehghani-Sanij A R, Dehghani S R, Naterer G F, et al. Sea spray icing phenomena on marine vessels and offshore structures: Review and formulation[J]. Ocean engineering, 2017, 132: 25-39.

Dehghani-Sanij A, Muzychka Y S, Naterer G F. Predicted ice accretion on horizontal surfaces of marine vessels and offshore structures in arctic regions[C]//International Conference on Offshore Mechanics and Arctic Engineering. American Society of Mechanical Engineers, 2016, 49996: V008T07A021.

DeNucci T, Brahan D, McGonagle P, et al. A time-dependent ice accretion model for trap-setting fishing vessels with filigree structures[C]//International Marine Design Conference. 2024.

Dhar S, Naseri M, Khawaja H A, et al. Design, development and deployment of a novel sea spray collector for sea-spray flux

measurements[J]. Cold Regions Science and Technology, 2024, 218: 104096.

Dombry C, Ferreira A. Maximum likelihood estimators based on the block maxima method[J]. 2019.

Faltinsen O. Sea loads on ships and offshore structures[M]. Cambridge university press, 1993.

Ferziger J H, Perić M, Street R L. Computational methods for fluid dynamics[M]. springer, 2019.

Horjen I, Loeset S, Vefsnmo S. Icing hazards on supply vessels and stand-by boats[R]. 1986.

Horjen I, Vefsnmo S. Mobile platform stability (MOPS). Subproject 02-icing (MOPS report No. 15)[J]. 1984.

Horjen I. Including partly freezing of droplets during flight in a sea spray icing model[J]. Ocean Engineering, 2024, 308: 118281.

Horjen I. Modeling of icing on a planar surface due to sea spray and blowing snow[J]. Ocean Engineering, 2023, 285: 115339.

IMO S. International code on intact stability[J]. 2008.

International Maritime Organization. International code for ships operating in polar waters (Polar Code)[J]. 2015.

International Towing Tank Conference (ITTC). Report of the Stability in Waves Committee[C]//Proceedings of 28th ITTC International Towing Tank Conference. 2017, 1: 275-335.

Jixiang Y, Tianying W, Wenyong T, et al. Roll Damping Prediction for a Three Dimensional Rectangle Floating Production Storage Offloading[J]. Journal of Shanghai Jiaotong University, 2018, 52(3): 261.

Johansen K, Sollid M P, Gudmestad O T. Stability of Vessels in an Ice-free Arctic[J]. TransNav: International Journal on Marine Navigation and Safety of Sea Transportation, 2020, 14.

Kang S, Song J. Parameter and quantile estimation for the generalized Pareto distribution in peaks over threshold framework[J]. Journal of the Korean Statistical Society, 2017, 46(4): 487-501.

Kubat I, Timco G. NRC Marine Icing Database[C]//Proceedings 11th International Workshop on Atmospheric Icing of Structures (IWAIS), XI, Montréal. 2005.

Liu Y. Research on numerical method of ship-roll chaos threshold[J]. Journal of Ship Mechanics, 2019, 23(2): 136-141.

Lozowski E P, Szilder K, Makkonen L. Computer simulation of marine ice accretion[J]. Philosophical Transactions of the Royal Society of London. Series A: Mathematical, Physical and Engineering Sciences, 2000, 358(1776): 2811-2845.

Lungu A. A Numerical Study of the Roll Damping for Double-Symmetric Bodies[J]. Procedia Manufacturing, 2020, 46: 475-483.

Makkonen L. Salinity and growth rate of ice formed by sea spray[J]. Cold Regions Science and Technology, 1987, 14(2): 163-171.

Mintu S, Molyneux D, Colbourne B. Full-scale SPH simulations of ship-wave impact generated sea spray[J]. Ocean Engineering, 2021, 241: 110077.

Mintu S, Molyneux D. Ice accretion for ships and offshore structures. Part 1-State of the art review[J]. Ocean Engineering, 2022, 258: 111501.

Naess A, Gaidai O, Karpa O. Estimation of extreme values by the average conditional exceedance rate method[J]. Journal of Probability and Statistics, 2013, 2013(1): 797014.

Naess A. Applied Extreme Value Statistics: With a Special Focus on the ACER Method[M]. Springer Nature, 2024.

Orimolade A P, Haver S, Gudmestad O T. Estimation of extreme significant wave heights and the associated uncertainties: A case study using NORA10 hindcast data for the Barents Sea[J]. Marine Structures, 2016, 49: 1-17.

Pipiras V. Pitfalls of data-driven peaks-over-threshold analysis: perspectives from extreme ship motions[J]. Probabilistic Engineering Mechanics, 2020, 60: 103053.

Preobrazhenskii L Y. Estimate of the content of spray drops in the near-water layer of the atmosphere[J]. 1973.

Rypkema D, Tuljapurkar S. Modeling extreme climatic events using the generalized extreme value (GEV) distribution[M]//Handbook of Statistics. Elsevier, 2021, 44: 39-71.

Samuelsen E M, Løset S, Edvardsen K. Marine icing observed on KV Nordkapp during a cold air outbreak with a developing polar low in the Barents sea[J]. 2015.

Samuelsen E M. Prediction of ship icing in Arctic waters-Observations and modeling for application in operational weather forecasting[J]. 2017.

SDC I M O. INF. 8 Annex 27 draft guidelines of direct stability assessment procedures as a part of the second generation intact stability criteria[J]. London: IMO, 2014.

Silva K M, Maki K J. Toward a computational fluid dynamics implementation of the critical wave groups method[J]. Ocean Engineering, 2021, 235: 109451.

Solas I M O. International convention for the safety of life at sea[J]. International Maritime Organization, 2003, 142.

Stallabrass J R. Trawler icing: A compilation of work done at NRC[M]. National Research Council Canada, 1980.

Üçer E. Lyapunov function based criteria for ship rolling in random beam seas[J]. Polish Maritime Research, 2019, 26(3): 6-14.

Wang Y, Perera L P, Batalden B M. Kinematic motion models based vessel state estimation to support advanced ship predictors[J]. Ocean Engineering, 2023, 286: 115503.

Xu S, Ji C, Soares C G. Short-term extreme mooring tension and uncertainty analysis by a modified ACER method with adaptive Markov Chain Monte Carlo simulations[J]. Ocean Engineering, 2021, 236: 109445.

Zhang Y, Luo G, Zhang Y, et al. A Review of Research on Ice Accumulation on Polar Ships[C]//International Conference on SmartRail, Traffic and Transportation Engineering. Singapore: Springer Nature Singapore, 2023: 623-632.

Zhou X, Li H, Huang Y, et al. New extreme statistics strategy for the extreme value predictions of ship parametric rolling motions through limited model test observations[J]. Ocean Engineering, 2023, 276: 114138.